

Noncovalent Z···Z (Z = O, S, Se, and Te) Interactions: How Do They Operate to Control Fine Structures of 1,8-Dichalcogene-Substituted Naphthalenes?

Satoko Hayashi and Waro Nakanishi*

Department of Material Science and Chemistry, Faculty of Systems Engineering, Wakayama University, 930 Sakaedani, Wakayama 640-8510

Received April 11, 2008; E-mail: nakanisi@sys.wakayama-u.ac.jp

Homonuclear Z···Z (Z = O, S, Se, and Te) interactions are investigated employing naphthalene 1,8-positions in 1,8-$(MeZ)_2C_{10}H_6$ (**1a–1d**: Z = O (**a**), S (**b**), Se (**c**), and Te (**d**)), 1-MeZ-8-$PhZC_{10}H_6$ (**2a–2c**), and 1,8-$(PhZ)_2C_{10}H_6$ (**3a–3d**). Three types of structures are detected for **1a–3d**: **BB** for **1a**, **CC** for **1b**, **1c**, **2c**, and **3d**, and **AB** for **2a**, **2b**, and **3a–3c**, in our definition, by X-ray crystallographic analysis, although some have already been reported. Quantum chemical calculations are performed on **1a–1d** and **3c**, together with model **c**, Me(H)Se···Se(H)Me, to elucidate how the fine structures are controlled by the interactions. **AB** are stabilized by the $n_p(Z)\cdots\sigma^*(Z–C)$ 3c–4e interactions for Z = S, Se, and Te. While **CC** are substantially stabilized by the $n(Z)\cdots\sigma^*(Z–C)$ interactions, they are well summarized as the disappearance of the nodal plane in $\pi^*(Z\cdots Z)$. Factors to control the fine structures are clarified and visualized using the HOMO or HOMO−1 of model **c**. The energy profile of model **c** helps us to imagine the whole picture of the noncovalent Se···Se interactions.

Much attention has been paid to weak interactions[1–13] because they determine fine structures of compounds and create high functionalities of materials. The interactions play an important role in structure, biological activity,[14] regulation of enzymatic functions,[15] stabilization of folded protein structures,[16] in supramolecular chemistry,[17] and in donor–acceptor complexes for electronic material.[18] They are also utilized as tools in crystal engineering for material development.[19] However, difficulty is often encountered in the detection of weak interactions and in demonstrating a cause and effect relation with phenomena arising from them because they are literally weak. Superficial factors can be mistaken for meaningful interactions, because they usually work behind other factors of superficial contribution. Each phenomenon in question should be analyzed as a result of the weak interaction, if it is the real cause. It is inevitable to set up a system for the establishment of the factors controlling the fine structures. It is also important to strengthen weak interactions for effective detection.

Several cases of orbital overlap in noncovalent Z···Z interactions of group 16 elements are shown in Scheme 1. Direct orbital overlap between nonbonded atoms will increase as the distance between the atoms in question become shorter. Therefore, close location and appropriate orientation of the orbitals are necessary for effective interactions.[4,8,20] Lone pair orbitals of group 16 elements cause versatile reactivities and give structurally interesting compounds.[21] To detect the weak interactions, the nonbonded atoms must be fixed within the sum of van der Waals radii[22] in an organic compound of rigid structure.[4,3a,23] Although severe exchange repulsions usually accompany the interactions,[4c–4f,23] they can be substantially decreased by placing the atoms at suitable positions and directions in a molecule.[4g,24]

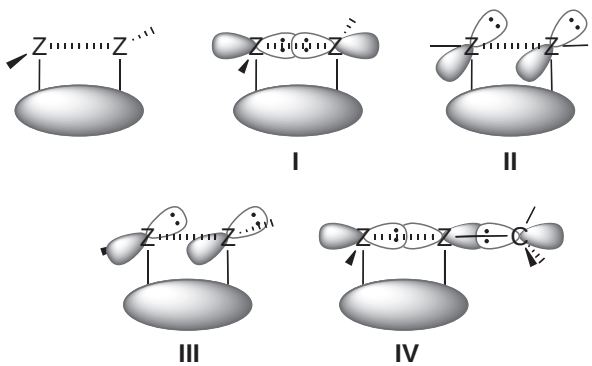

Scheme 1. Noncovalent interactions caused by direct orbital overlaps. **I**: σ(2c–4e), **II**: π(2c–4e), **III**: distorted π(2c–4e), and **IV**: σ(3c–4e).

Naphthalene 1,8-positions provide a good system to study noncovalent interactions,[2–4,8,23,25] since the distances between the nonbonded heteroatoms at these positions are close to van der Waals radii minus one Å for main group elements.[4b,4d–4g,4i,8,25] Weak noncovalent interactions gain covalent nature as the nonbonded distances decrease relative to the sum of van der Waals radii. Interactions between nonbonded atoms at naphthalene 1,8-positions may contain both characteristics depending on Z. Noncovalent homonuclear Z···Z (Z = O, S, Se, and Te) interactions are thoroughly investigated, aiming to clarify the whole picture of the noncovalent interactions at naphthalene 1,8-positions. To clarify the cause-and-effect in weak interactions is another purpose of our investigations.[10]

1,8-Dichalcogene-substituted naphthalenes, 1,8-$(MeZ)_2$-$C_{10}H_6$ (**1a–1d**: Z = O (**a**), S (**b**), Se (**c**), and Te (**d**)), 1-MeZ-

Published on the web December 12, 2008; doi:10.1246/bcsj.81.1605

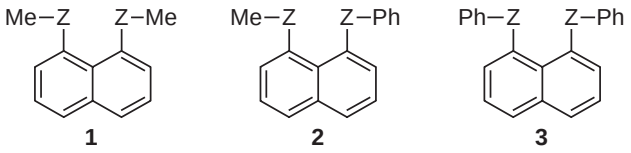

(Z = O (**a**), S (**b**), Se (**c**), and Te (**d**))

Chart 1. 1,8-Dichalcogene-substituted naphthalenes **1**–**3**.

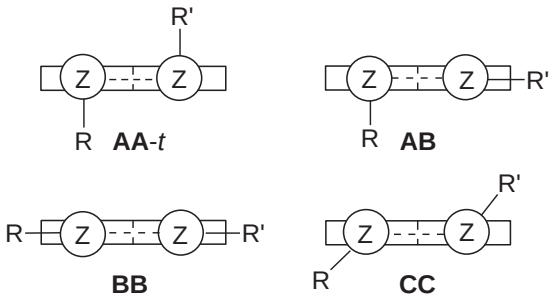

Scheme 2. Typical structures in **1**–**3**.

8-PhZC$_{10}$H$_6$ (**2a**–**2c**), and 1,8-(PhZ)$_2$C$_{10}$H$_6$ (**3a**–**3d**) are employed for the investigations (Chart 1): **1d** and **2d** were not prepared successfully, which may be due to the facile cleavage of the Te–C$_{Me}$ bonds in the compounds. Structures of **1a**–**1c**, **2a**–**2c**, and **3a**–**3d** (**1a**–**3d**) were determined by X-ray crystallographic analysis, although **1a**,[26] **1b**,[2b] **2c**,[4e,4g] **3b**,[27] and **3d**[3a] have already been reported.

The structures around Z in 8-G-1-RZC$_{10}$H$_6$ are well described as three types, **A** (**A**), **B**, and **C**, where the Z–C$_R$ bond is perpendicular to the naphthyl plane in **A**, it is on the plane in **B**, and **C** is intermediate between **A** and **B**.[4c,4d,4f–4i,5b] Scheme 2 illustrates typical structures for 1-RZ-8-R′ZC$_{10}$H$_6$, **AA**-*t* (**AA** pairing of the trans conformation), **BB**, **AB**, and **CC**.[4g] The **BB** structure was reported for **1a**[26] by Sternhell et al., **CC** for **1b**[2b] by Glass et al., and for **3d**[3a] by Furukawa et al. We investigated the structure of **2c**, which was also **CC** and a successive change was observed by changing the substituent at the phenyl p position in **2c**.[4e–4g]

Fine structures of **1a**–**3d** were analyzed to understand how they are controlled by weak interactions and how the weak interactions operate to determine the fine structures. They were analyzed from the viewpoint of noncovalent homonuclear Z···Z interactions at the naphthalene 1,8-positions, together with the p–π conjugations of p(Z)···π(Nap) and/or p(Z)···π(Ph) (p(Z)···π(Nap/Ph)). Results of quantum chemical (QC) calculations are reported for donor–acceptor interactions in Me$_2$Z···Z′RMe (Z, Z′ = O, S, Se, and Te; R = Me and CN).[28] However, it is also important to clarify the factors that control the fine structure in the real compounds, **1a**–**3d**. QC calculations were performed on **1a**–**1d** and **3c** to analyze the results and elucidate the mechanisms to control the fine structures. QC calculations were also performed on model **c** (Me(H)Se···Se(H)Me), devised based on the observed structures of **1c** to visualize the factors and to imagine the whole picture of the interactions.

Here, we report the structures of **1a**–**3d**, although some have already been reported. Factors controlling fine structures are clarified. The noncovalent homonuclear Z···Z interactions

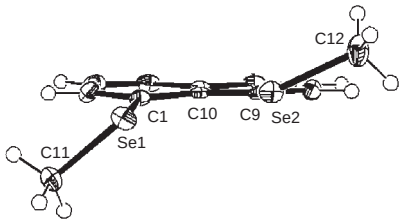

Figure 1. ORTEP drawing of **1c**$_A$ with atomic numbering scheme for selected atoms (50% probability thermal level).

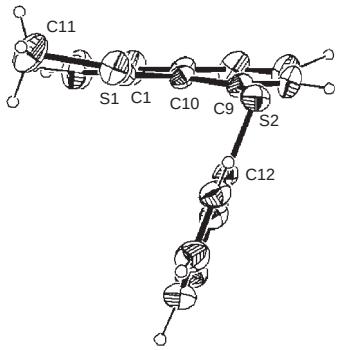

Figure 2. ORTEP drawing of **2b** with atomic numbering scheme for selected atoms (50% probability thermal level).

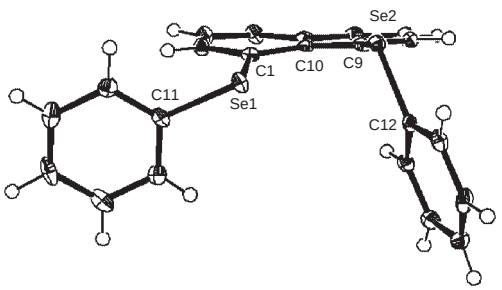

Figure 3. ORTEP drawing of **3c** with atomic numbering scheme for selected atoms (50% probability thermal level).

(Z = O, S, Se, and Te) are the main factors, together with p(Z)···π(Nap/Ph) conjugations, although the crystal packing effect must also be considered.

Results and Discussion

Structures of 1–3. Single crystals were obtained for **1b**–**3c** via slow evaporation of hexane solutions. The X-ray crystallographic analyses were carried out for a suitable crystal of each compound. Although the structures of **1a**,[26] **1b**,[2b] **2c**,[4e,4g] **3b**,[27] and **3d**[3a] have already been reported, that of **3b** was reexamined to improve refinement. While one structure corresponds to **2b** and **3a**–**3c**, two correspond to **1a**–**1c**, **2a**, and **2c** in the crystals. Figures 1–3 show the structures of **1c**$_A$, **2b**, and **3c**, respectively. Those of **1c**$_B$, **2a**$_A$, **2a**$_B$, **3a**, and **3b** are shown in the Supporting Information (SI) (Figures S1–S4, respectively). Table 1 displays selected interatomic distances, angles, and torsional angles, necessary for discussion.

Table 1. Nonbonded Z···Z Distances, Angles, and Torsional Angles around Z, Observed in **1–3**

Z = O

	1a$_A$ [a]	**1a**$_B$ [a]	**2a**$_A$	**2a**$_B$	**3a**
Temp[b]	RT	RT	103 K	103 K	103 K
r/Å[c]	2.543	2.547	2.590(3)	2.604(3)	2.616(9)
Δr/Å[d]	−0.50	−0.49	−0.45	−0.44	−0.42
θ_1/°[e]	117.23	117.26	115.7(3)	116.8(4)	118.05(12)
θ_2/°[f]	117.23	117.26	118.0(3)	117.7(3)	117.76(13)
θ_3/°[g]	152.65	152.70	151.4(3)	151.0(3)	148.26(12)
θ_4/°[h]	152.65	152.70	93.2(3)	93.4(3)	83.91(12)
ϕ_1/°[i]	−179.85	−179.34	174.5(3)	−174.8(3)	169.28(13)
ϕ_2/°[j]	−179.85	−179.34	94.0(4)	−93.8(4)	−82.92(19)
Structure	**BB**	**BB**	**AB**	**AB**	**AB**

Z = S

	1b$_A$ [k]	**1b**$_B$ [k]	**2b**	**3b**[l]	**3b**[m]
Temp[b]	RT	RT	RT	RT	RT
r/Å[c]	2.918	2.936	3.047(2)	3.004	3.021(2)
Δr/Å[d]	−0.68	−0.66	−0.55	−0.60	−0.58
θ_1/°[e]	103.9	101.5	103.1(2)	102.46	102.4(2)
θ_2/°[f]	103.6	103.3	104.9(2)	102.67	104.2(2)
θ_3/°[g]	155.4	151.9	172.8(2)	168.52	165.0(2)
θ_4/°[h]	168.3	162.6	80.7(1)	105.07	91.9(1)
ϕ_1/°[i]	−143.2	−142.1	171.9(3)	−159.99	−152.1(4)
ϕ_2/°[j]	−158.3	−153.0	69.5(4)	−95.25	101.7(4)
Structure	**CC**	**CC**	**AB**	**AB**	**AB**

Z = Se

	1c$_A$	**1c**$_B$	**2c**$_A$ [n]	**2c**$_B$ [n]	**3c**
Temp[b]	103 K	103 K	RT	RT	103 K
r/Å[c]	3.051(4)	3.064(4)	3.091(1)	3.048(1)	3.135(2)
Δr/Å[d]	−0.75	−0.74	−0.71	−0.75	−0.67
θ_1/°[e]	99.29(16)	98.41(16)	98.2(4)	97.8(4)	97.80(8)
θ_2/°[f]	99.27(16)	98.50(16)	98.1(3)	98.4(3)	99.15(9)
θ_3/°[g]	164.47(3)	146.46(3)	140.2(3)	148.6(4)	171.32(9)
θ_4/°[h]	150.34(3)	159.73(3)	156.5(3)	157.6(2)	95.87(8)
ϕ_1/°[i]	−154.1(3)	136.8(3)	122.4(3)	−133.0(7)	−154.74(16)
ϕ_2/°[j]	−138.8(3)	148.0(3)	141.8(3)	−143.2(6)	109.70(16)
Structure	**CC**	**CC**	**CC**	**CC**	**AB**

a) Ref. 26. b) Temperature for measurements. c) r(Z1, Z2). d) r(Z1, Z2) − Σr_{vdW}(Z). e) ∠C1Z1C11. f) ∠C9Z2C12. g) ∠Z2Z1C11. h) ∠Z1Z2C12. i) ∠C10C1Z1C11. j) ∠C10C9Z2C12. k) Ref. 2b. l) Ref. 27. m) Reexamined data in this work. n) Refs. 4e and 4g.

Scheme 3 summarizes the structures of **1a–3c** determined in this work, together with those reported in the literature. The **CC** structure of **3d**[3a] is also contained in Scheme 3. Three structures are observed for **1a–3d**: **BB** for **1a**, **CC** for **1b**, **1c**, **2c**, and **3d**, and **AB**[29] for **2a**, **2b**, and **3a–3c**, as shown in Figures 1–3 and Scheme 3. The structures of **1d** and **2d** are yet unknown, since they have not been prepared successfully perhaps due to facile cleavage of the Te–C_{Me} bonds during preparation.[30] The **CC** structure is strongly suggested for **1d** by QC calculations: **1d** (**CC**) is optimized even starting from **1d** (**AB**), which will be discussed latter (Table 2). The structure of **1d** (**CC**) is displayed in Scheme 3. Scheme 3 demonstrates that the three types of structures distribute systematically along with the feature size of molecules, if the structure of **1d** and **2d** are supposed to the both **CC**.

Table 1 displays selected interatomic distances, angles, and torsional angles, necessary for discussion. Differences between the observed O···O distances and the sum of the van der Waals radii[22a] in **1a** (**BB**) ($\Delta r(O,O) = r_{obsd}(O,O) - 2r_{vdW}(O)$) are −0.50 to −0.49 Å. The magnitudes seem to have little affect on the structure of **1a**, although the p lone pair orbitals ($n_p(O)$) would overlap to some extent at those distances. Instead, the p–π conjugation of p(O)–π(Nap) must be much stronger than the $n_p(O)\cdots n_p(O)$ interaction in **1a** (**BB**). The p(O)–π(Nap) conjugation places the O–C_{Me} bonds on the naphthyl plane, which must be the main factor controlling the structure of **1a** (**BB**). The Δr values in **2a** (**AB**) and **3a** (**AB**) are −0.45 and −0.42 Å, respectively. One may suppose that the noncovalent $n_p(O)\cdots\sigma^*$(O–C) 3c–4e interaction plays an important role to determine **AB** in **2a** and **3a**, at first glance.

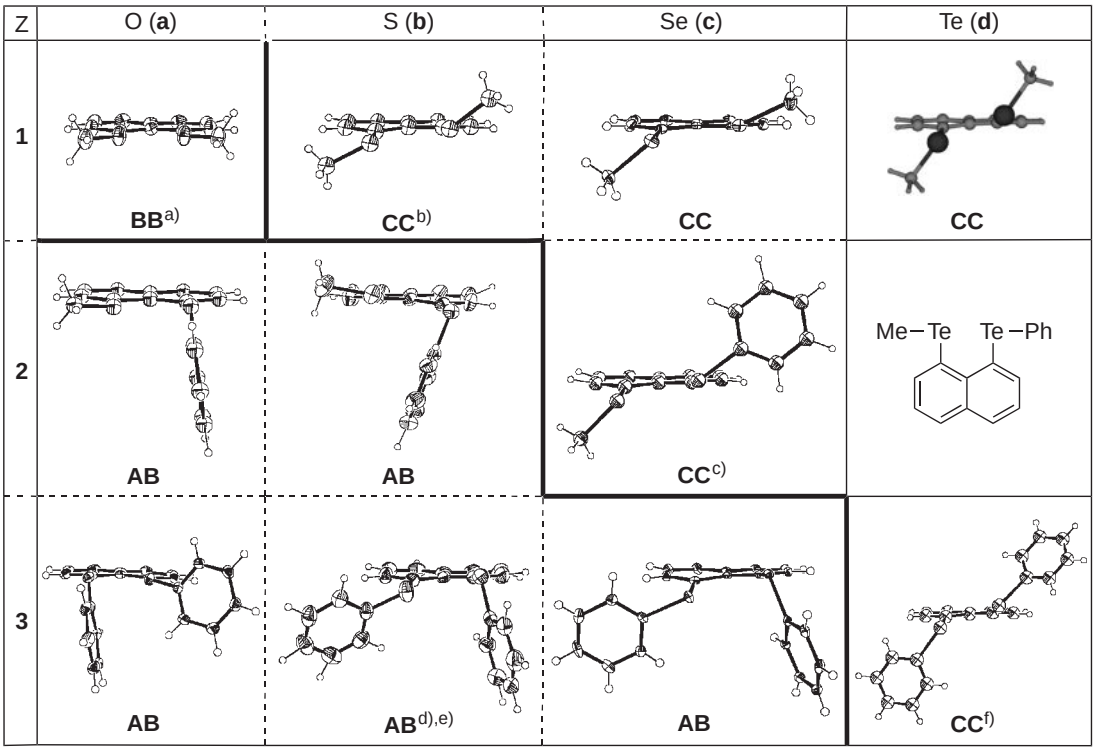

a) Ref. 26. b) Ref. 2b. c) Refs. 4e and 4g. d) Ref. 27. e) Reexamined. f) Ref. 3a.

Scheme 3. Observed structures in **1a**–**3d**.

However, **AB** appears without the noncovalent O···O interaction. The p(O)–π(Ph) conjugation may control **AB** of **2a** and **3a**,[31] in addition to the p(O)–π(Nap) conjugation. Namely, the structures of **2a** (**AB**) and **3a** (**AB**) are determined mainly by the p(O)–π(Nap/Ph) conjugations.

The importance of the noncovalent Z···Z interaction becomes larger as Z = O goes to S then to Se and further to Te, whereas the p(Z)–π(Nap/Ph) conjugations decrease in the order Z = O $\gg$ S > Se > Te. The noncovalent S···S interaction has greater effect on the structure of **1b** (**CC**) with Δr(S, S) of -0.67 Å. **CC** forms when **BB** is distorted, where π(2c–4e) is also distorted in **CC**. Namely, the distorted π(2c–4e) interaction must operate to determine the structure of **1b** (**CC**). The Δr(S, S) values of **2b** (**AB**) and **3b** (**AB**) are -0.55 and -0.59 Å, respectively, which are smaller than that in **1b** (**CC**) by ca. 0.10 Å. The noncovalent n_p(S)···σ^*(S–C) 3c–4e interaction must play an important role in stabilizing the structures of **2b** (**AB**) and **3b** (**AB**), with the assistance of the p(S)–π(Nap/Ph) conjugations.

In the case of Z = Se, Δr(Se, Se) of **1c** (**CC**) and **2c** (**CC**) are -0.75 and -0.73 Å, respectively, and that of **3c** (**AB**) is -0.67 Å. The values in **CC** are smaller than those in **AB** by 0.06–0.08 Å. Distorted π(2c–4e) interaction operates to determine the structures of **1c** (**CC**) and **2c** (**CC**) as in **1b** (**CC**). The structure of **3c** (**AB**) must be the result of noncovalent n_p(Se)···σ^*(Se–C) 3c–4e interaction, together with the p(Se)–π(Nap/Ph) conjugations. The Te···Te distance in **3d** (**CC**) is reported to be 3.135 Å, where $\Delta r(\mathrm{Te,Te}) = -0.67$ Å for **3d** (**CC**). However, we must be careful when the Δr(Z, Z) values are discussed, since they are not determined mainly by the magnitude of the Z···Z interactions.[32]

Why are such systematic distributions observed in **1a**–**3d** as shown in Scheme 3? QC calculations were performed to analyze the factors controlling the fine structures, although the crystal packing effect must also play an important role to determine the structures.

QC Calculations. QC calculations were performed on **1a**–**1d** and **3c**.[33,34] Calculations were performed both at the density functional theory (DFT) level of the Becke three parameter hybrid functionals with the Lee–Yang–Parr correlation functional (B3LYP)[35–37] and the Møller–Plesset second order energy correlation (MP2) method.[38–40] The 6-311+G(2d,p) basis sets of Gaussian 03[41] were employed for the calculations of **1a**–**1c** at the DFT (B3LYP) level. The DGDZVP basis sets[42] were employed for Te with the 6-311+G(2d,p) basis sets for C and H in the calculations of **1d** at DFT (B3LYP) level. The 6-311+G(d) basis sets were employed for O, S, and Se with the 6-31G(d) basis sets for C and H in the calculations of **1a**–**1c** and the DGDZVP basis sets[42] were employed for all nuclei in **1d** at the MP2. Frequency analysis was carried out on all optimized structures of **1a**–**1d**. The B3LYP/6-311+G(2d,p) method was applied to the calculations of **3c**. Similarly, 6-311+G(d) basis sets were employed for Se with the 4-31G(d) basis sets for C and H in the calculations of **3c** at the MP2 level. Frequency analysis was not performed on **3c**.

Scheme 4 shows model **c** (Me(H)Se···Se(H)Me) devised based on the structure of **1c**.[43] The energy profile for model **c** is examined to visualize the factors controlling the fine structures and to imagine the whole picture of the noncovalent Se···Se interactions. Calculations were performed with the MP2/6-311+G(3d,2p) method.

Table 2. Results of QC Calculations on **1a–1d**[a)]

	AA-*t* (C_2)	**AB** (C_1)	**BB** (C_{2v})	**CC** (C_2)
At the DFT (B3LYP) level[b)]				
1a				
r(O···O)/Å	2.7576	2.6525	2.5492	—[c)]
E(F)/au	−614.9307	−614.9332	−614.9350	—[c)]
ΔE(F)/kJ mol^{-1}	0.0[d)]	−6.6	−11.3	—[c)]
1b				
r(S···S)/Å	3.2684	3.0316	(2.9374)[e)]	2.9374[f)]
E(F)/au	−1260.8999	−1260.9038	(−1260.8973)[e)]	−1260.9012
ΔE(F)/kJ mol^{-1}	0.0[d)]	−10.2	(6.8)[e)]	−3.4
1c				
r(Se···Se)/Å	3.4364	3.1553	(3.0747)[e)]	3.1038
E(F)/au	−5267.5589	−5267.5647	(−5267.5568)[e)]	−5267.5657
ΔE(F)/kJ mol^{-1}	0.0[d)]	−15.2	(5.5)[e)]	−17.9
1d				
r(Te···Te)/Å	3.6936	—[g)]	(3.3541)[e)]	3.3724
E(F)/au	−13691.6431	—[g)]	(−13691.6394)[e)]	−13691.6511
ΔE(F)/kJ mol^{-1}	0.0[d)]	—[g)]	(9.7)[e)]	−21.0
At the MP2 level[h)]				
1a				
r(O···O)/Å	—[i)]	2.6508	2.5296	—[c)]
E(F)/au	—[i)]	−612.8726	−612.8730	—[c)]
ΔE(F)/kJ mol^{-1}	—[i)]	0.0[d)]	−1.1	—[c)]
1b				
r(S···S)/Å	—[i)]	3.0592	—[i)]	3.0601
E(F)/au	—[i)]	−1258.0809	—[i)]	−1258.0806
ΔE(F)/kJ mol^{-1}	—[i)]	0.0[c)]	—[i)]	0.8
1c				
r(Se···Se)/Å	—[i)]	3.1664	—[i)]	3.1587
E(F)/au	—[i)]	−5262.8721	—[i)]	−5262.8729
ΔE(F)/kJ mol^{-1}	—[i)]	0.0[d)]	—[i)]	−2.1
1d				
r(Te···Te)/Å	3.6828	—[g)]	—[i)]	3.4022
E(F)/au	−13684.8452	—[g)]	—[i)]	−13685.8528
ΔE(F)/kJ mol^{-1}	0.0[d)]	—[g)]	—[i)]	−20.0

a) Energies containing the sum of electronic and thermal Gibbs free energies at 298.15 K are given by E(F) (and ΔE(F)). b) The 6-311+G(2d,p) basis sets are employed for **1a–1c** and the DGDZVP basis sets for Te with the 6-311+G(2d,p) basis sets in the calculations of **1d**. c) Optimized to be **BB**, when starting from **CC**. d) Taken as the standard. e) Corresponding to the species with two imaginary frequencies. f) **CC** (C_1) with all positive frequencies which are very close to **CC** (C_2) with only one negative (imaginary) frequency for each. See also Ref. 44. g) Optimized to be **CC** when starting from **AB**. h) The 6-311+G(d) basis sets are employed for O, S, and Se with the 6-31G(d) basis sets for C and H in the calculations of **1a–1c** and the DGDZVP basis sets[42] are employed for all nuclei in **1d**. i) Not calculated.

Indeed, structures and energies evaluated on the basis of QC calculations essentially correspond to those in the gas phase, but the factors controlling and stabilizing structures in the gas phase must also operate in solid state. Other factors such as the crystal packing effect in crystals are stronger than those predicted by QC calculations for molecules. However, it is expected that such structures would be preferentially observed that are substantially stabilized in the gas phase even if the crystal packing effect operates. Therefore, it is instructive to examine those predicted by QC calculations as incentive factors to control fine structures while they are not so predominant.

Results of Calculations on 1a–1d and 3c. Table 2 shows the energies containing thermal corrections to Gibbs free energy at 298.15 K (E(F)) for **1a–1d**, together with the energy differences (ΔE(F)). Table 2 also contains the optimized Z···Z distances for **1a–1d**. Table 3 shows the energies on the potential energy surface (E) for **3c**, together with the energy differ-

ences (ΔE). Table 2 (3) also contains the optimized Z···Z distances for **3a**. Table 3 also contains the data of **1c** for convenience of comparison.

For **1a**, **AA**-*t* (C_2), **AB** (C_1), and **BB** (C_{2v}) are optimized to be stable, while **BB** is optimized even when starting from **CC**, based on DFT calculations. The three structures are demonstrated to be the energy minima by the frequency analysis of **1a** (see also Table S1 in the SI). **BB** is a global minimum containing a thermal correction to Gibbs free energy at 298.15 K (and on the potential energy surface). The observed **1a** (**BB**) is well explained by the QC calculations.

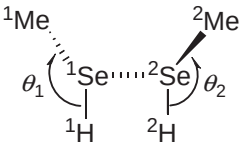

θ_1: $\angle^1H^1Se^1C$, θ_2: $\angle^2H^2Se^2C$

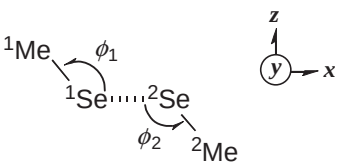

ϕ_1: $\angle^2Se^1H^1Se^1C$, ϕ_2: $\angle^1Se^2H^2Se^2C$

Scheme 4. Model **c**.

On the other hand, **AA**-*t* (C_2), **AB** (C_1), and **CC** (C_2)[44] are energy minima, whereas **BB** (C_{2v}) is not for **1b** and **1c**[45] (see also Tables S2 and S3 in the SI). **CC** and **AB** would be in equilibrium in solutions for **1b** and **1c**. **1c** (**CC**) is predicted to be the global minimum, which explains well the observed results.[46] While **1b** (**AB**) is calculated to be more stable than **1b** (**CC**), the energy difference is very small when calculated at the MP2 level ($\Delta E = E(\mathbf{CC}) - E(\mathbf{AB}) = 0.8\,\mathrm{kJ\,mol^{-1}}$). The crystal packing effect controls the subtle energy balance for the structures of **1b** in crystals. In the case of **1d**, **AA**-*t* (C_2) and **CC** (C_2)[44] are optimized to be stable (see also Table S4 in the SI). **1d** (**CC**) must be the global minimum, since **1d** (**AB**) converges to **1d** (**CC**), starting from **1d** (**AB**), and **1d** (**CC**) is substantially more stable than **1d** (**AA**). Results of MP2 calculations well support the observed structures, although the calculations are limited to the important conformers of **AB** (C_1) and **BB** (C_{2v}) for **1a**, **AB** (C_1) and **CC** (C_2) for **1b** and **1c**, and **AA** (C_2) and **CC** (C_2) for **1d**.[47]

While **1c** (**AB**) is calculated to be more stable than **1c** (**CC**) by 1.1 kJ mol^{-1}, **3c** (**AB**) is predicted to be more stable than **3c** (**CC**) by 5.8 kJ mol^{-1} on the potential energy surface at the MP2 level. Therefore, the energy difference between **3c** (**AB**) and **3c** (**CC**) is predicted to be larger than the case of **1c** (**AB**)/**1c** (**CC**) by 4.7 kJ mol^{-1} at the MP2 level. The energy difference between **3c** (**AB**)/**3c** (**CC**) is also predicted to be smaller than **1c** (**AB**)/**1c** (**CC**) at the B3LYP level, although **CC** are predicted to more stable in this case. These results explain well the preferential **AB** conformer in **3c** relative to the case of **1c**.

Table 3. Results of QC Calculations on **1c** and **3c**[a)]

	AA-*t* (C_2)	**AB** (C_1)	**BB** (C_{2v})	**CC** (C_2)
B3LYP				
1c[b),c)]				
r(Se···Se)/Å	3.4364	3.1553	(3.0747)[d)]	3.1038
E/au	−5267.7173	−5267.7219	(−5267.7182)[d)]	−5267.7211
ΔE/kJ mol^{-1}	0.0[e)]	−12.1	(−2.4)[d)]	−10.0
3c[b)]				
r(Se···Se)/Å	3.4129	3.1568	(3.0798)[f)]	3.1104
E/au	−5651.2863	−5651.2917	(−5651.2882)[f)]	−5651.2922
ΔE/kJ mol^{-1}	0.0[e)]	−14.3	(−5.0)[f)]	−15.5
MP2				
1c[c),g)]				
r(Se···Se)/Å	—[h)]	3.1664	—[h)]	3.1587
E/au	—[h)]	−5263.0316	—[h)]	−5263.0312
ΔE/kJ mol^{-1}	—[h)]	0.0[e)]	—[h)]	1.1
3c[i)]				
r(Se···Se)/Å	—[h)]	3.1670	—[h)]	3.1222
E/au	—[h)]	−5643.2775	—[h)]	−5643.2753
ΔE/kJ mol^{-1}	—[h)]	0.0[e)]	—[h)]	5.8

a) Energies on the potential energy surface are given by E. b) The 6-311+G(2d,p) basis sets being employed. c) The same structures shown in Table 2. d) Corresponding to the species with two imaginary frequencies. e) Taken as the standard. f) Should correspond to the species with two imaginary frequencies, although frequency analysis was not performed. g) The 6-311+G(d) basis sets employed for Se with the 6-31G(d) basis sets for C and H. h) Not calculated. i) The 6-311+G(d) basis sets employed for Se with the 4-31G(d) basis sets for C and H.

After observation of the fine structures caused by the noncovalent Z···Z interactions in the naphthalene system, together with analysis based on QC calculations, the next extension is to exhibit the whole picture of the interactions and visualize the factors.

Energy Profile for Model c. To imagine the whole picture of the noncovalent Se···Se interactions, the energy profile for model **c** (Z = Se) is examined. The potential energy surfaces are calculated by optimizing model **c** with ϕ_1 fixed suitably. The (ϕ_1, ϕ_2) values of **AA**-*t*, **AB**, **BB**, and **CC** are employed as the starting values. Figure 4 draws the energy profile for model **c** calculated with the MP2/6-311+G(3d,2p) method, which demonstrates how the noncovalent Z···Z interactions act as the factors to determine the fine structures. **CC** is predicted to be the global minimum and **AB** is the next global minimum. They are on the same energy surface. **AA**-*t* (C_2) with $(\phi_1, \phi_2) = (87.5°, 87.5°)$ is predicted to be a local minimum on another energy surface. **AA**-*t* becomes less stable as the structure is deformed then it assimilates into the energy surface leading to **AB** and **CC** at around $(\phi_1, \phi_2) = (60.0°, 177.5°)$ and $(140.0°, 164.3°)$.

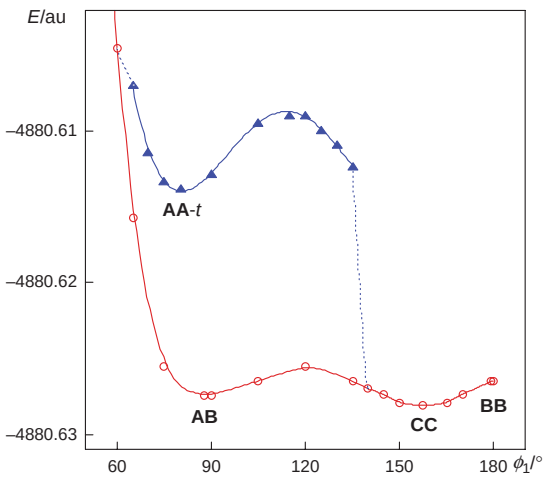

Figure 4. Plots of E versus ϕ_1 in model **c**, calculated with the MP2/6-311+G(3d,2p) method.

Factors to Control the Structures. Factors controlling the fine structures are visualized exemplified by model **c**. Scheme 5 draws the HOMO and HOMO−1 of **AA**-*t*, **AB**, **BB**, and **CC** in model **c**, calculated with the MP2/6-311+G(3d,2p) method. The orbital interactions imply factors based on specific structures. Factors controlling the fine structures are summarized as shown below, although the role of the p(Z)–π(Nap/Ph) conjugations must also be considered in the real compounds, especially for Z = O.

1. The double p(O)–π(Nap) conjugations determine the structure of **1a** (**BB**). The p(Z)–π(Nap) conjugations in **BB** become weaker in the order Z = O > S > Se > Te.

2. The hypervalent $n_p(Z)\cdots\sigma^*(Z–C)$ 3c–4e interactions (Z = S, Se, and Te) operate in **AB**, which stabilize the system. The p(Z)–π(Nap/Ph) conjugations also support stabilization of **AB**.

3. **CC** is formed by the distortion of **BB**. The donor–acceptor interactions of $n_s(Z)\cdots\sigma^*(Z–C)$ and $n_p(Z)\cdots\sigma^*(Z–C)$ substantially stabilize **CC**. The disappearance of the nodal plane in π^*(Z···Z: HOMO) in **CC** contributes to stabilize **CC**, where the nodal plane appears apparently in **BB**. The relative stability of **CC** increase in the order Z = O ≪ S < Se < Te.

4. **AA**-*t* is constructed by σ(2c–4e). **AA**-*t* of the symmetric structure is a local minimum. The stability decreases as **AA**-*t* becomes unsymmetrical.

Factors to control the structures of **1**–**3** are well visualized in Scheme 5, as summarized above.

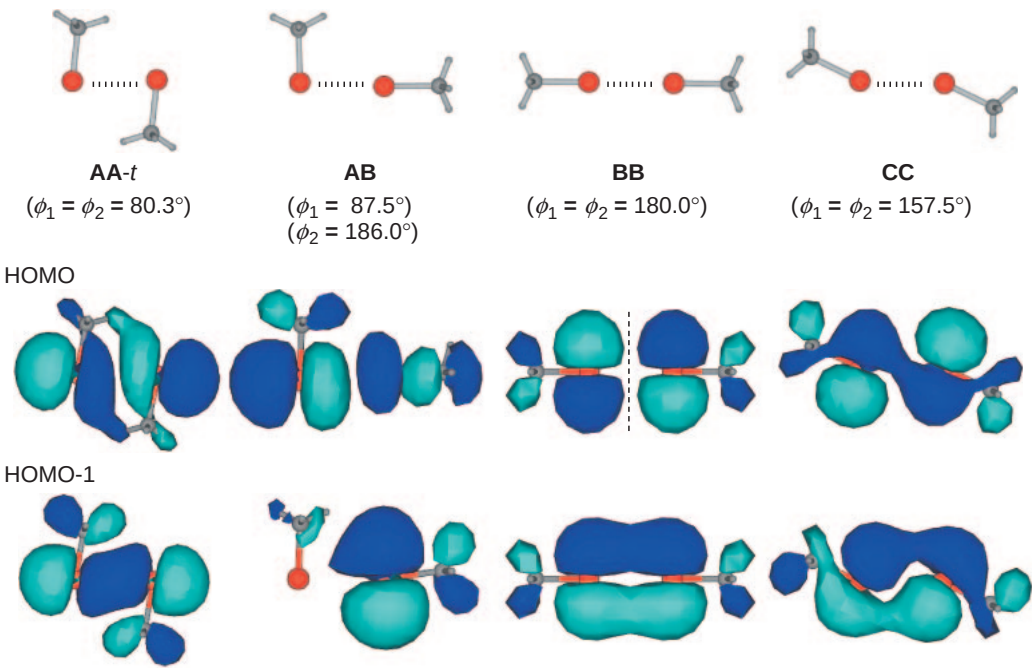

Scheme 5. HOMO and HOMO−1 of **AA**-*t*, **AB**, **BB**, and **CC** in model **c**.

Conclusion

Weak interactions determine fine structures of molecules and create high functionalities of materials. We investigated weak interactions originating from orbital overlap as the first step to establish the cause-and-effect in weak interactions. It is inevitable to set up a system so as to analyze each phenomenon in question as the result of the weak interactions. Weak noncovalent interactions become weakly covalent. Homonuclear Z···Z interactions were investigated, employing 1,8-$(MeZ)_2$-$C_{10}H_6$ (**1a**–**1d**), 1-MeZ-8-$PhZC_{10}H_6$ (**2a**–**2c**), and 1,8-$(PhZ)_2$-$C_{10}H_6$ (**3a**–**3d**). It was elucidated how the fine structures of **1a**–**3d** are controlled by the weak interactions and how weak interactions act to determine the fine structures, after determination of the structures by X-ray crystallographic analysis.

QC calculations were performed on **1a**–**1d** and **3c**, together with model **c** at both B3LYP and MP2 levels. Factors to control the fine structures of **1a**–**3d**, caused by noncovalent $n_p(Z)\cdots n_p(Z)$ interactions, were established based on experimental and theoretical investigations. **AB** and **CC** are the most important structures for Z = S and Se. **AB** and **CC** must also be important for Z = Te although **1a** (**AB**) optimized to **1a** (**CC**) in the QC calculations. **AB** is stabilized by $n_p(Z)\cdots\sigma^*(Z–C)$ 3c–4e interactions and **CC** is stabilized by both $n_s(Z)\cdots\sigma^*(Z–C)$ and $n_p(Z)\cdots\sigma^*(Z–C)$ interactions. It can also be briefly stated that **CC** is stabilized with the disappearance of the nodal plane in π^*(Z···Z: HOMO) in **CC**, apparently appearing in **BB**. The energy profile of model **c** helps us to imagine the whole picture of the noncovalent $n_p(Z)\cdots n_p(Z)$ interactions. The factors are visualized employing the HOMO or HOMO−1 of model **c**.

Superficial factors are sometimes mistakenly identified as sources of fine structure in systems where weak interactions play an important role, since weak interactions usually work behind other factors of superficial contribution. Such cases are found even in the literature. A firm guideline is necessary for the phenomena caused by the weak interactions. The above results will supply one such guideline, which will enable the study of more insights into the phenomena caused by weak interactions.

Investigations on the role of the noncovalent heteronuclear Z···Z′ interactions (Z, Z′ = O, S, Se, and Te) are in progress. The results will be reported elsewhere.

Experimental

General. Manipulations were performed under an argon atmosphere with standard vacuum-line techniques. Glassware was dried at 130 °C overnight. Solvents and reagents were purified by standard procedures as necessary. The melting points were determined on a Yanako MP-S3 melting point apparatus and are uncorrected. NMR spectra were recorded at 25 °C on a JEOL AL-300 spectrometer (^{1}H, 300 MHz; ^{13}C, 75 MHz) and JEOL Lambda-400 spectrometer (^{77}Se, 76 MHz). The ^{1}H, ^{13}C, and ^{77}Se chemical shifts are given in parts per million relative to those of Me_4Si and external MeSeMe, respectively. Flash column chromatography was performed with 400-mesh silica gel and basic alumina and analytical thin layer chromatography was performed on precoated silica gel plates (60F-254) with the systems (v/v) indicated.

1,8-Bis(methylselanyl)naphthalene (1c). To a solution which was prepared by reduction of naphtho[1,8-*c*,*d*]-1,2-diselenole[48] with $NaBH_4$ in an aqueous THF solution, was added methyl iodide at room temperature. After a usual workup, the crude was chromatographed on silica gel containing basic alumina. Recrystallization of the chromatographed product from hexane gave **1c** as colorless prisms in 98% yield, mp 85.0–85.5 °C; ^{1}H NMR (300 MHz, $CDCl_3$, 23 °C, TMS): δ 2.33 (s, 6H), 7.32 (t, J = 7.7 Hz, 2H), 7.70 (dd, J = 1.2 and 8.2 Hz, 2H), 7.73 (dd, J = 1.2 and 7.5 Hz, 2H); ^{13}C NMR (75 MHz, $CDCl_3$, 23 °C, TMS): δ 13.3, 125.7, 128.3, 131.9, 132.3, 135.3, 135.6; ^{77}Se NMR (76 MHz, $CDCl_3$, 23 °C, MeSeMe): δ 234.06; elemental analysis: Calcd for $C_{12}H_{12}Se_2$ (314.14): C 45.88, H 3.85%. Found: C, 45.73; H, 3.77%.

1-Methoxy-8-phenoxynaphthalene (2a).[49] To a 2,4,6-trimethylpyridine solution of phenol, was added 1-iodo-8-methoxynaphthalene[50] and copper I oxide. The solution was refluxed for 4 h under argon atmosphere. After usual work-up, the crude product was chromatographed on silica gel containing basic alumina and gave **2a** as colorless prisms in 95% yield; mp 97–98 °C; ^{1}H NMR (300 MHz, $CDCl_3$, 23 °C, TMS): δ 3.65 (s, 3H), 6.77 (dt, J = 1.0 and 7.6 Hz, 1H), 6.82 (dd, J = 1.1 and 7.5 Hz, 2H), 6.96 (dt, J = 1.1 and 7.3 Hz, 1H), 7.10 (dd, J = 1.1 and 7.5 Hz, 1H), 7.24 (dd, J = 7.4 and 8.5 Hz, 2H), 7.37 (t, J = 7.8 Hz, 1H), 7.42 (t, J = 7.6 Hz, 1H), 7.46 (dd, J = 1.3 and 8.3 Hz, 1H), 7.65 (dd, J = 1.1 and 8.3 Hz, 1H); ^{13}C NMR (75 MHz, $CDCl_3$, 23 °C, TMS): δ 55.9, 106.1, 116.0, 119.0, 119.9, 120.7, 121.1, 125.0, 126.5, 126.5, 129.3, 137.5, 151.2, 155.9, 160.1; elemental analysis: Calcd for $C_{17}H_{14}O_2$ (250.29): C, 81.58; H, 5.64%. Found: C, 81.60; H, 5.64%.

1-Methylthio-8-phenylthionaphthalene (2b). To a solution which was prepared by reduction of bis(8-phenylthionaphthyl)-1,1′-disulfide[51] with NaH in DMF solution at 70 °C, was added methyl iodide at room temperature. After a usual workup, the crude was chromatographed on silica gel containing basic alumina. Recrystallization of the chromatographed product from hexane gave **2b** as colorless prisms in 96% yield, mp 52.0–53.0 °C; ^{1}H NMR (300 MHz, $CDCl_3$, 23 °C, TMS): δ 2.50 (s, 3H), 7.12–7.19 (m, 3H), 7.20–7.27 (m, 2H), 7.34 (t, J = 7.7 Hz, 1H), 7.39–7.44 (m, 2H), 7.59 (dd, J = 1.3 and 7.3 Hz, 1H), 7.66 (dd, J = 3.5 and 5.9 Hz, 1H), 7.79 (dd, J = 1.3 and 8.3 Hz, 1H); ^{13}C NMR (75 MHz, $CDCl_3$, 23 °C, TMS): δ 19.8, 125.8, 126.2, 126.3, 126.7, 129.1, 129.4, 130.0, 132.1, 133.0, 135.6, 135.9, 137.7, 139.3; elemental analysis: Calcd for $C_{17}H_{14}S_2$ (282.42): C, 72.30; H, 5.00%. Found: C, 72.06; H, 5.04%.

1,8-Diphenoxynaphthalene (3a).[49] To a 2,4,6-trimethylpyridine solution of phenol, was added an 1,8-diiodonaphthalene[52] and copper I oxide. The solution was refluxed for 10 h under argon atmosphere. After usual work-up, the crude product was chromatographed on silica gel containing basic alumina and gave **3a** as colorless prisms in 68% yield; mp 84–85 °C; ^{1}H NMR (300 MHz, $CDCl_3$, 23 °C, TMS): δ 6.64–6.68 (m, 4H), 6.93–6.98 (m, 2H), 7.01 (dd, J = 0.7 and 7.3 Hz, 2H), 7.14–7.22 (m, 2H), 7.42 (t, J = 7.9 Hz, 2H), 7.66–7.72 (m, 4H); ^{13}C NMR (75 MHz, $CDCl_3$, 23 °C, TMS): δ 117.1, 117.7, 121.9, 124.5, 126.6, 129.3, 137.7, 151.3, 158.8; elemental analysis: Calcd for $C_{22}H_{16}O_2$ (312.36): C, 84.59; H, 5.16%. Found: C, 84.53; H, 5.07%.

1,8-Bis(phenylthio)naphthalene (3b).[27] To a 2,4,6-trimethylpyridine solution of benzenethiol, was added 1,8-diiodonaphthalene[52] and copper I oxide. The solution was refluxed for 10 h under argon atmosphere. After usual work-up, the crude product was

chromatographed on silica gel containing basic alumina and gave **3b** as colorless prisms in 94% yield; mp 68–69 °C; ^{1}H NMR (300 MHz, $CDCl_3$, 23 °C, TMS): δ 7.16–7.31 (m, 10H), 7.32 (t, $J = 7.6$ Hz, 2H), 7.47 (dd, $J = 1.5$ and 7.3 Hz, 2H), 7.76 (dd, $J = 1.5$ and 8.1 Hz, 2H); ^{13}C NMR (75 MHz, $CDCl_3$, 23 °C, TMS): δ 125.8, 126.7, 129.1, 129.2, 131.0, 133.1, 133.8, 134.0, 136.1, 138.5; elemental analysis: Calcd for $C_{22}H_{16}S_2$: C, 76.70; H, 4.68%. Found: C, 76.53; H, 4.71%.

1,8-Bis(phenylselanyl)naphthalene (3c). To a DMF solution of diphenyl diselenide, was added NaH under argon atmosphere. The mixture was held at 110 °C for 30 min, then to it was added 1,8-diiodonaphthalene[52] and copper I oxide. The solution was held at 140 °C for 12 h under argon atmosphere. After usual work-up, the crude product was chromatographed on silica gel containing basic alumina and gave **3c** as pale yellow needles in 59% yield; mp 64.0–64.8 °C; ^{1}H NMR (300 MHz, $CDCl_3$, 23 °C, TMS): δ 7.22–7.28 (m, 8H), 7.39–7.45 (m, 4H), 7.64 (dd, $J = 1.1$ and 7.3 Hz, 2H), 7.74 (dd, $J = 1.1$ and 8.3 Hz, 2H); ^{13}C NMR (75 MHz, $CDCl_3$, 23 °C, TMS): δ 126.0, 127.4, 129.2, 129.4, 131.4, 133.4, 135.18, 135.19, 135.5, 135.9; ^{77}Se NMR (76 MHz, $CDCl_3$, 23 °C, MeSeMe): δ 435.4; elemental analysis: Calcd for $C_{22}H_{16}Se_2$ (438.28): C, 60.29; H, 3.68%. Found: C, 60.21; H, 3.75%.

X-ray Crystal Structural Determination. The crystals of **1c**, **2a**, **2b**, **3a**, **3b**, and **3c** were grown by slow evaporation of dichloromethane–hexane solutions at room temperature. The intensity data were collected on a CCD diffractometer equipped with graphite-monochromed Mo Kα radiation ($\lambda = 0.71070$ Å) at 103(2) K for **1c**, **2a**, **3a**, and **3c** and on a four-circle diffractometer with graphite-monochromated Mo Kα radiation ($\lambda = 0.71069$ Å) for **2b**, and **3b** at 298(1) K. The structures of **1c**, **2a**, **3a**, and **3c** were solved by direct method (SIR97)[53] and refined by full-matrix least-square method on F^2 for all reflections (SHELXL-97).[54] The structures were solved by Patterson interpretation using the program DIRDIF92[55] for **2b** and **3b** and by and refined by full-matrix least-square techniques. All the non-hydrogen atoms were refined anisotropically. CCDC-640537 for **1c**, CCDC-640538 for **2a**, CCDC-640539 for **2b**, CCDC-640540 for **3a**, CCDC-640591 for **3b**, and CCDC-640541 for **3c** contain the supplementary crystallographic data for this paper. These data can be obtained free of charge from the Cambridge Crystallographic Data Centre via www.ccdc.cam.ac.uk/data_request/cif.

We are grateful to Prof. Norihiro Tokitoh and Dr. Takahiro Sasamori, Institute for Chemical Research, Kyoto University, for the X-ray diffraction measurements of **1c**, **2a**, **3a**, and **3c**. This work was partially supported by a Grant-in-Aid for Scientific Research (Nos. 16550038 and 19550041) from the Ministry of Education, Culture, Sports, Science and Technology, Japan.

Supporting Information

ORTEP drawing of $\mathbf{1c}_B$, $\mathbf{2a}_A$, $\mathbf{2a}_B$, **3a**, and **3b** are shown in Figures S1–S4, respectively. Results of QC calculations by frequency analysis on **1a**–**1d** are shown in Tables S1–S4, respectively. Optimized structures given by Cartesian coordinates for **1a**–**1d**, **3c**, and model **c**, together with the total energies and the method for the calculations. These materials are available free of charge on the web at http://www.csj.jp/journals/bcsj/.

References

1 a) *Molecular Interactions. From van der Waals to Strongly Bound Complexes*, ed. by S. Scheiner, Wiley, New York, **1997**. b) K. D. Asmus, *Acc. Chem. Res.* **1979**, *12*, 436. c) W. K. Musker, *Acc. Chem. Res.* **1980**, *13*, 200. d) A. Kucsman, I. Kapovits, *Non-Bonded Sulfur-Oxygen Interaction in Organic Sulfur Compounds* in *Organic Sulfur Compounds in Organic Sulfur Chemistry: Theoretical and Experimental Advances*, ed. by F. Bernardi, I. G. Csizmadia, A. Mangini, Elsevier, Amsterdam, **1985**, Chap. 4.

2 a) R. S. Glass, S. W. Andruski, J. L. Broeker, *Rev. Heteroat. Chem.* **1988**, *1*, 31. b) R. S. Glass, S. W. Andruski, J. L. Broeker, H. Firouzabadi, L. K. Steffen, G. S. Wilson, *J. Am. Chem. Soc.* **1989**, *111*, 4036. c) R. S. Glass, L. Adamowicz, J. L. Broeker, *J. Am. Chem. Soc.* **1991**, *113*, 1065.

3 a) H. Fujihara, H. Ishitani, Y. Takaguchi, N. Furukawa, *Chem. Lett.* **1995**, 571. b) N. Furukawa, K. Kobayashi, S. Sato, *J. Organomet. Chem.* **2000**, *611*, 116.

4 a) W. Nakanishi, *Chem. Lett.* **1993**, 2121. b) W. Nakanishi, S. Hayashi, S. Toyota, *Chem. Commun.* **1996**, 371. c) W. Nakanishi, S. Hayashi, H. Yamaguchi, *Chem. Lett.* **1996**, 947. d) W. Nakanishi, S. Hayashi, A. Sakaue, G. Ono, Y. Kawada, *J. Am. Chem. Soc.* **1998**, *120*, 3635. e) W. Nakanishi, S. Hayashi, S. Toyota, *J. Org. Chem.* **1998**, *63*, 8790. f) S. Hayashi, W. Nakanishi, *J. Org. Chem.* **1999**, *64*, 6688. g) W. Nakanishi, S. Hayashi, T. Uehara, *J. Phys. Chem. A* **1999**, *103*, 9906. h) W. Nakanishi, S. Hayashi, *J. Org. Chem.* **2002**, *67*, 38. i) S. Hayashi, H. Wada, T. Ueno, W. Nakanishi, *J. Org. Chem.* **2006**, *71*, 5574.

5 a) W. Nakanishi, S. Hayashi, H. Kihara, *J. Org. Chem.* **1999**, *64*, 2630. b) W. Nakanishi, S. Hayashi, T. Uehara, *Eur. J. Org. Chem.* **2001**, 3933.

6 a) M. Iwaoka, S. Tomoda, *J. Am. Chem. Soc.* **1994**, *116*, 4463. b) M. Iwaoka, S. Tomoda, *J. Am. Chem. Soc.* **1996**, *118*, 8077. c) H. Komatsu, M. Iwaoka, S. Tomoda, *Chem. Commun.* **1999**, 205.

7 *Chemistry of Hypervalent Compounds*, ed. by K.-y. Akiba, Wiley-VCH, New York, **1999**.

8 W. Nakanishi, *Hypervalent Chalcogen Compounds* in *Handbook of Chalcogen Chemistry: New Perspectives in Sulfur, Selenium and Tellurium*, ed. by F. A. Devillanova, Royal Society of Chemistry, Cambridge, **2006**, Chap. 10.3.

9 R. E. Rosenfield, Jr., R. Parthasarathy, J. D. Dunitz, *J. Am. Chem. Soc.* **1977**, *99*, 4860.

10 G. R. Desiraju, T. Steiner, *The Weak Hydrogen Bond in Structural Chemistry and Biology; International Union of Crystallography Monographs on Crystallography*, Oxford University Press, Oxford, **1999**, *9*, 507.

11 T. Steiner, *Angew. Chem., Int. Ed.* **2002**, *41*, 48; K. Müller-Dethlefs, P. Hobza, *Chem. Rev.* **2000**, *100*, 143; P. R. Mallinson, G. T. Smith, C. C. Wilson, E. Grech, K. Wozniak, *J. Am. Chem. Soc.* **2003**, *125*, 4259; G. P. Schiemenz, S. Pörksen, P. M. Dominiak, K. Wozniak, *Z. Naturforsch., B: Chem. Sci.* **2002**, *57*, 8.

12 C. Bleiholder, D. B. Werz, H. Köppel, R. Gleiter, *J. Am. Chem. Soc.* **2006**, *128*, 2666; C. Bleiholder, R. Gleiter, D. B. Werz, H. Köppel, *Inorg. Chem.* **2007**, *46*, 2249.

13 C. Réthoré, A. Madalan, M. Fourmigué, E. Canadell, E. B. Lopes, M. Almeida, R. Clérac, N. Avarvari, *New J. Chem.* **2007**, *31*, 1468.

14 a) F. T. Burling, B. M. Goldstein, *J. Am. Chem. Soc.* **1992**, *114*, 2313. b) Y. Nagao, T. Hirata, S. Goto, S. Sano, A. Kakehi, K. Iizuka, M. Shiro, *J. Am. Chem. Soc.* **1998**, *120*, 3104. c) S. Wu, A.

Greer, *J. Org. Chem.* **2000**, *65*, 4883. d) Y. Nagao, H. Iimori, S. Goto, T. Hirata, S. Sano, H. Chuman, M. Shiro, *Tetrahedron Lett.* **2002**, *43*, 1709. e) E. Meyer, A. C. Joussef, H. Gallardo, A. J. Bortoluzzi, R. L. Longo, *Tetrahedron* **2003**, *59*, 10187. f) Y. Nagao, T. Honjo, H. Iimori, S. Goto, S. Sano, M. Shiro, K. Yamaguchi, Y. Sei, *Tetrahedron Lett.* **2004**, *45*, 8757.

15 J. C. Taylor, G. D. Markham, *J. Biol. Chem.* **1999**, *274*, 32909; W. Brandt, A. Golbraikh, M. Täger, U. Lendeckel, *Eur. J. Biochem.* **1999**, *261*, 89.

16 a) M. Iwaoka, S. Takemoto, M. Okada, S. Tomoda, *Chem. Lett.* **2001**, 132. b) M. Iwaoka, S. Takemoto, M. Okada, S. Tomoda, *Bull. Chem. Soc. Jpn.* **2002**, *75*, 1611.

17 G. R. Desiraju, *Angew. Chem.* **1995**, *107*, 2541; *Angew. Chem., Int. Ed. Engl.* **1995**, *34*, 2311.

18 V. Lippolis, F. Isaia, *Charge-Transfer (C.-T.) Adducts and Related Compounds* in *Handbook of Chalcogen Chemistry: New Perspectives in Sulfur, Selenium and Tellurium*, ed. by F. A. Devillanova, Royal Society of Chemistry, Cambridge, **2006**, Chap. 8.2: C. Réthoré, M. Fourmigué, N. Avarvari, *Chem. Commun.* **2004**, 1384; C. Réthoré, M. Fourmigué, N. Avarvari, *Tetrahedron* **2005**, *61*, 10935; C. Réthoré, N. Avarvari, E. Canadell, P. Auban-Senzier, M. Fourmigué, *J. Am. Chem. Soc.* **2005**, *127*, 5748.

19 T. Suzuki, H. Fujii, Y. Yamashita, C. Kabuto, S. Tanaka, M. Harasawa, T. Mukai, T. Miyashi, *J. Am. Chem. Soc.* **1992**, *114*, 3034; M. Turbiez, P. Frére, M. Allain, C. Videlot, J. Ackermann, J. Roncali, *Chem.—Eur. J.* **2005**, *11*, 3742; A. F. Cozzolino, I. Vargas-Baca, S. Mansour, A. H. Mahmoudkhani, *J. Am. Chem. Soc.* **2005**, *127*, 3184.

20 a) G. C. Pimentel, *J. Chem. Phys.* **1951**, *19*, 446; J. I. Musher, *Angew. Chem.* **1969**, *81*, 68; *Angew. Chem., Int. Ed. Engl.* **1969**, *8*, 54. b) M. M. L. Chen, R. Hoffmann, *J. Am. Chem. Soc.* **1976**, *98*, 1647. c) P. A. Cahill, C. E. Dykstra, J. C. Martin, *J. Am. Chem. Soc.* **1985**, *107*, 6359. See also: R. A. Hayes, J. C. Martin, *Sulfurane Chemistry* in *Organic Sulfur Chemistry: Theoretical and Experimental Advances*, ed. by F. Bernardi, I. G. Csizmadia, A. Mangini, Elsevier, Amsterdam, **1985**. d) N. C. Baenziger, R. E. Buckles, R. J. Maner, T. D. Simpson, *J. Am. Chem. Soc.* **1969**, *91*, 5749.

21 a) *The Chemistry of the Ether Linkage*, ed. by S. Patai, Wiley, New York, **1967**; *The Chemistry of The Thiol Group*, ed. by S. Patai, Wiley, New York, **1974**, Vols. 1 and 2; *The Chemistry of Ethers, Crown Ethers, Hydroxy Groups and Their Sulphur Analogues, Suppl. E*, ed. by S. Patai, Wiley, New York, **1980**, Vols. 1 and 2; *The Chemistry of Organic Selenium and Tellurium Compounds*, ed. by S. Patai, Z. Rappoport, Wiley, New York, **1986**, Vol. 1; *The Chemistry of Organic Selenium and Tellurium Compounds*, ed. by S. Patai, Wiley, New York, **1986**, Vol. 2. b) *Organic Chemistry of Sulfur*, ed. by S. Oae, Plenum Press, New York, **1977**. c) *Organic Sulfur Chemistry: Theoretical and Experimental Advances*, ed. by F. Bernardi, I. G. Csizmadia, A. Mangini, Elsevier, Amsterdam, **1985**. d) *Organic Selenium Compounds: Their Chemistry and Biology*, ed. by D. L. Klayman, W. H. H. Günther, Wiley, New York, **1973**. e) *Organic Selenium Chemistry*, ed. by D. Liotta, Wiley-Interscience, New York, **1987**; *The Organic Chemistry of Tellurium*, ed. by K. J. Irgolic, Gordan and Breach Science Publishers, New York, **1974**. f) *Organoselenium Chemistry, A Practical Approach*, ed. by T. G. Back, Oxford University Press, Oxford, **1999**. g) *Tellurium-Containing Heterocycles*, ed. by M. R. Detty, M. B. O'Regan, Wiley, New York, **1994**, see also references cited therein.

22 a) A. Bondi, *J. Phys. Chem.* **1964**, *68*, 441. b) L. Pauling, *J. Am. Chem. Soc.* **1947**, *69*, 542. c) *The Nature of the Chemical Bond*, 3rd ed., ed. by L. Pauling, Cornell University Press, Ithaca, New York, **1960**, Chap. 7.

23 a) H. Fujihara, M. Yabe, J.-J. Chiu, N. Furukawa, *Tetrahedron Lett.* **1991**, *32*, 4345; N. Furukawa, T. Fujii, T. Kimura, H. Fujihara, *Chem. Lett.* **1994**, 1007. b) H. Fujihara, R. Saito, M. Yabe, N. Furukawa, *Chem. Lett.* **1992**, 1437. c) I. Johannsen, H. Eggert, *J. Am. Chem. Soc.* **1984**, *106*, 1240; I. Johannsen, H. Eggert, S. Gronowitz, A.-B. Hörnfeldt, *Chem. Scr.* **1987**, *27*, 359; H. Fujihara, H. Mima, T. Erata, N. Furukawa, *J. Am. Chem. Soc.* **1992**, *114*, 3117.

24 H. Margenau, *Phys. Rev.* **1939**, *56*, 1000; **1943**, *64*, 131; J. O. Hirschfelder, J. W. Linnett, *J. Chem. Phys.* **1950**, *18*, 130; N. Moore, *J. Chem. Phys.* **1960**, *33*, 471; A. Van der Avoird, *Chem. Phys. Lett.* **1967**, *1*, 24.

25 a) G. Gafner, *Acta Crystallogr.* **1962**, *15*, 1081. b) M. A. Davydova, Yu. T. Struchkow, *Zh. Strukt. Khim.* **1962**, *3*, 184. c) M. A. Davydova, Yu. T. Struchkow, *Zh. Strukt. Khim.* **1968**, *9*, 258. d) H. Bock, M. Sievert, Z. Havlas, *Chem.—Eur. J.* **1998**, *4*, 677. e) R. D. Jackson, S. James, A. G. Orpen, P. G. Pringle, *J. Organomet. Chem.* **1993**, *458*, C3.

26 R. Cosmo, T. W. Hambley, S. Sternhell, *Acta Crystallogr., Sect. B* **1990**, *46*, 557.

27 P. Nagy, D. Szabó, I. Kapovits, A. Kucsman, G. Argay, A. Kálman, *J. Mol. Struct.* **2002**, *606*, 61.

28 C. Bleiholder, R. Gleiter, D. B. Werz, H. Köppel, *Inorg. Chem.* **2007**, *46*, 2249.

29 One might wonder that the determination of **AB** seems sometimes unclear, since the Z_1–C_1 and Z_8–C_8 bonds in 1,8-$(PhZ)_2C_{10}H_6$ deviate out of the naphthalene plane. In such case, **AB** is identified by $\angle Z_8Z_1C_i$ and $\angle Z_1Z_8C_{i'}$ being close to 90 and 180°, respectively.

30 Efforts were also made to determine the structures of **1d** and **2d** but as of yet have not been successful, due to their instability. The structures are expected to be also **CC**, judging from the **CC** of **1c** and **2c**.

31 The $n_p(Z)\cdots\sigma^*(Z–C)$ interactions seem not to be effective for Z = O and the $n_p(Z)\cdots\sigma^*(Z–H)$ interactions are not effective maybe due to the weak accepting ability of $\sigma^*(Z–H)$.

32 Details of the factors to control the Z···Z distances will be reported elsewhere.

33 The energy differences due to the conformers around the $Se–C_{Ar}$ bonds in 1-MeSeNap and MeSePh are calculated at both MP2 and DFT levels. The results are closely related to the p–π conjugation of p(Se)–π(Nap/Ph), which will be reported elsewhere.[32]

34 The **AB** conformers play a crucial role in the heteronuclear Z···Z′ interactions at naphthalene 1,8-positions. The role of the phenyl group(s) will be discussed again in the Z···Z′ interactions.

35 C. Lee, W. Yang, R. G. Parr, *Phys. Rev. B* **1988**, *37*, 785; B. Miehlich, A. Savin, H. Stoll, H. Preuss, *Chem. Phys. Lett.* **1989**, *157*, 200.

36 A. D. Becke, *Phys. Rev. A* **1988**, *38*, 3098; A. D. Becke, *J. Chem. Phys.* **1993**, *98*, 5648.

37 The DFT level is also employed to optimize the structures here. However, the DFT level should be carefully employed when the system contains noncovalent interactions. DFT would not evaluate the noncovalent interactions correctly, since DFT with most functionals are not treated by the exchange-correlation functional. See, also Ref. 12.

38 M. Head-Gordon, J. A. Pople, M. J. Frisch, *Chem. Phys. Lett.* **1988**, *153*, 503; M. J. Frisch, M. Head-Gordon, J. A. Pople,

Chem. Phys. Lett. **1990**, *166*, 275; M. J. Frisch, M. Head-Gordon, J. A. Pople, *Chem. Phys. Lett.* **1990**, *166*, 281; M. Head-Gordon, T. Head-Gordon, *Chem. Phys. Lett.* **1994**, *220*, 122.

39 S. Sæbø, J. Almlöf, *Chem. Phys. Lett.* **1989**, *154*, 83.

40 C. Møller, M. S. Plesset, *Phys. Rev.* **1934**, *46*, 618; J. Gauss, *J. Chem. Phys.* **1993**, *99*, 3629; J. Gauss, *Ber. Bunsen-Ges. Phys. Chem.* **1995**, *99*, 1001.

41 M. J. Frisch, G. W. Trucks, H. B. Schlegel, G. E. Scuseria, M. A. Robb, J. R. Cheeseman, J. A. Montgomery, Jr., T. Vreven, K. N. Kudin, J. C. Burant, J. M. Millam, S. S. Iyengar, J. Tomasi, V. Barone, B. Mennucci, M. Cossi, G. Scalmani, N. Rega, G. A. Petersson, H. Nakatsuji, M. Hada, M. Ehara, K. Toyota, R. Fukuda, J. Hasegawa, M. Ishida, T. Nakajima, Y. Honda, O. Kitao, H. Nakai, M. Klene, X. Li, J. E. Knox, H. P. Hratchian, J. B. Cross, V. Bakken, C. Adamo, J. Jaramillo, R. Gomperts, R. E. Stratmann, O. Yazyev, A. J. Austin, R. Cammi, C. Pomelli, J. W. Ochterski, P. Y. Ayala, K. Morokuma, G. A. Voth, P. Salvador, J. J. Dannenberg, V. G. Zakrzewski, S. Dapprich, A. D. Daniels, M. C. Strain, O. Farkas, D. K. Malick, A. D. Rabuck, K. Raghavachari, J. B. Foresman, J. V. Ortiz, Q. Cui, A. G. Baboul, S. Clifford, J. Cioslowski, B. B. Stefanov, G. Liu, A. Liashenko, P. Piskorz, I. Komaromi, R. L. Martin, D. J. Fox, T. Keith, M. A. Al-Laham, C. Y. Peng, A. Nanayakkara, M. Challacombe, P. M. W. Gill, B. Johnson, W. Chen, M. W. Wong, C. Gonzalez, J. A. Pople, *Gaussian 03, Revision D.02*, Gaussian, Inc., Wallingford CT, **2004**.

42 The standard basis of DGDZVP is (5D, 7F) and the AO basis sets for Te are (633321/53321/531).

43 Two Se atoms in model **c** are placed on the *x*-axis with the Se···Se distances fixed at the observed values and two Se–H bonds are in the *z*-directions with $\angle^2\mathrm{Se}^1\mathrm{Se}^1\mathrm{H} = \angle^1\mathrm{Se}^2\mathrm{Se}^2\mathrm{H} = 90.0^\circ$. Consequently, the four atoms are placed in the *xz* plane, for each. The torsional angle of $^1\mathrm{H}^1\mathrm{Se}^2\mathrm{Se}^2\mathrm{H}$ (ϕ) is fixed at zero.

44 Although **CC** (C_2) is the desirable structure for **1c**, the structure gives one negative (imaginary) frequency for an internal motion after the frequency analysis. Instead, **1c** (**CC**: C_1), which is very similar to **1c** (**CC**: C_2), gave positive frequencies for all internal motions by the frequency analysis.

45 Motions with lower frequencies (-45.1, -67.2, and $-76.6\,\mathrm{cm}^{-1}$ for **1b–1d**, respectively) generate **CC** from **BB**. However, those with second lower values (-5.1, -19.5, and $-26.7\,\mathrm{cm}^{-1}$ for **1b–1d**, respectively) correspond to the rotation around the C_{2v} axis in **BB** maintaining the plane for the four C_{Me}, Z, Z, and C_{Me} atoms (Z = S, Se, or Te) with the naphthyl plane moving inverse direction.

46 The factor to stabilize **CC** is called Möbius stabilization, although **CC** is not cyclic. See Ref. 4f.

47 The r(Z···Z) values become larger in the order r(**BB**) < r(**CC**) < r(**AB**) ≪ r(**AA**-*t*), which must also be accounted for based on the weak interactions.

48 J. Meinwald, D. Dauplaise, J. Clardy, *J. Am. Chem. Soc.* **1977**, *99*, 7743.

49 R. G. R. Bacon, O. J. Stewart, *J. Chem. Soc.* **1965**, 4953.

50 P. C. Bell, W. Skranc, X. Formosa, J. O'Leary, J. D. Wallis, *J. Chem. Soc., Perkin Trans. 2* **2002**, 878.

51 W. Nakanishi, S. Hayashi, T. Arai, *Chem. Commun.* **2002**, 2416.

52 B. Bossenbroek, D. C. Sanders, H. M. Curry, H. Shechter, *J. Am. Chem. Soc.* **1969**, *91*, 371; H. O. House, D. G. Koepsell, W. J. Campbell, *J. Org. Chem.* **1972**, *37*, 1003.

53 A. Altomare, M. C. Burla, M. Camalli, G. L. Cascarano, C. Giacovazo, A. Guagliardi, A. G. G. Moliterni, G. Polidori, R. Spagna, *J. Appl. Crystallogr.* **1999**, *32*, 115.

54 G. M. Sheldrick, *SHELXL-97, Program for the Refinement of Crystal Structures*, University of Göttingen, Göttingen, **1997**.

55 P. T. Beurskens, G. Admiraal, G. Beurskens, W. P. Bosman, S. Garcia-Granda, R. O. Gould, J. M. M. Smits, C. Smykalla, *DIRDIF92, The DIRDIF Program System, Technical Report of the Crystallography Laboratory*, University of Nijmegen, The Netherlands, **1992**.